Electronic Supplementary Information (ESI) for

Self-floating hybrid hydrogels assembled with conducting polymer hollow spheres and silica aerogel microparticles for solar steam generation

Mengyao Tan,[a,b,§] Jin Wang,[b,§] Wenhui Song,[c] Jianhui Fang,[a] and Xuetong Zhang[b,c*]*

[a] Department of Chemistry, College of Sciences, Shanghai University, Shanghai 200444, P. R. China

[b] Suzhou Institute of Nano-Tech and Nano-Bionics, Chinese Academy of Sciences, Suzhou 215123, P. R. China

[c] Department of Surgical Biotechnology, Division of Surgery & Interventional Science, University College London, London, NW3 2PF, UK

[*]E-mail: (XZ) xtzhang2013@sinano.ac.cn; (JF) jhfang@shu.edu.cn

[§] These authors contributed equally

Figures of the Supporting Information

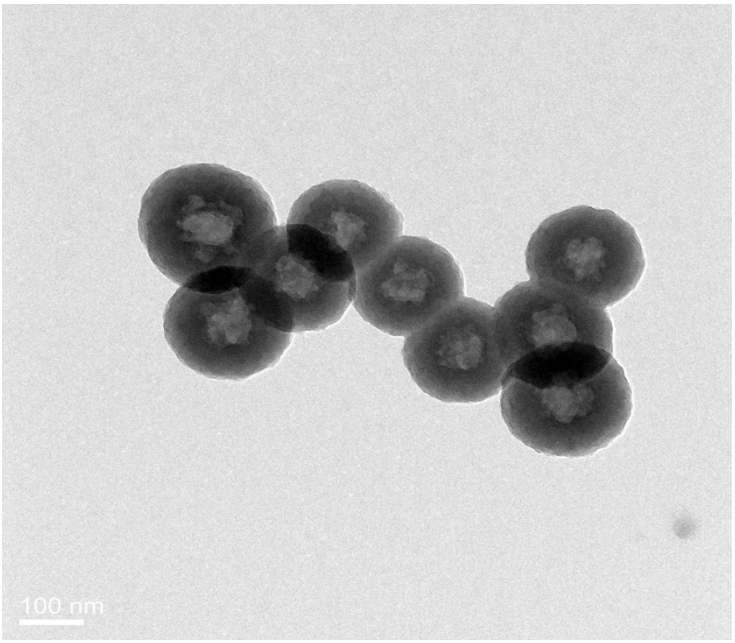

Fig. S1 TEM image of the CPHS used in this work.

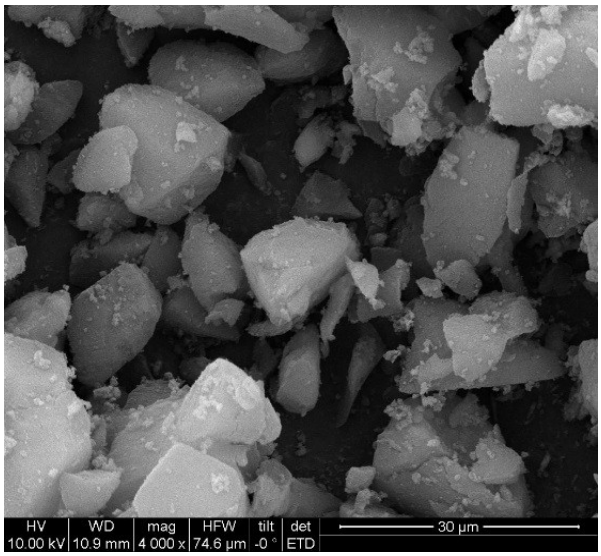

Fig. S2 SEM image of the silica aerogel microparticles.

(a)

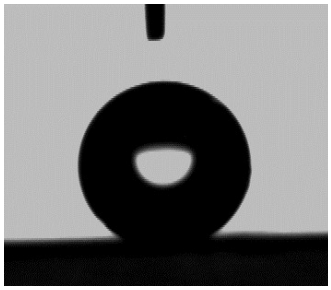

(b)

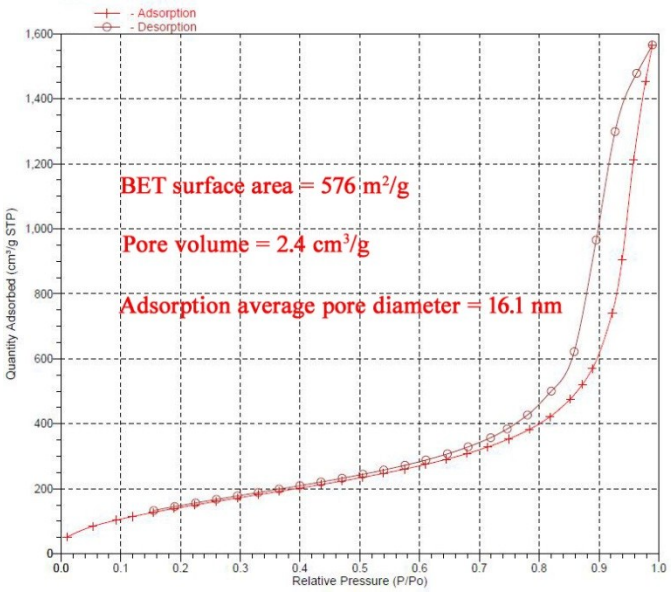

Fig. S3 (a) contact angle of the silica aerogels (149 ^{0}); (b) N_2 adsorption and desorption curve of the silica aerogel.

Fig. S4 PVA composite hydrogel with 15 wt.% of aerogel microparticles.

Fig. S5 photo image of the CPHS/aerogel functional PVA hydrogel, the hydrogel can self-float on deionized water. The volume of the deionized water was 33 ml.

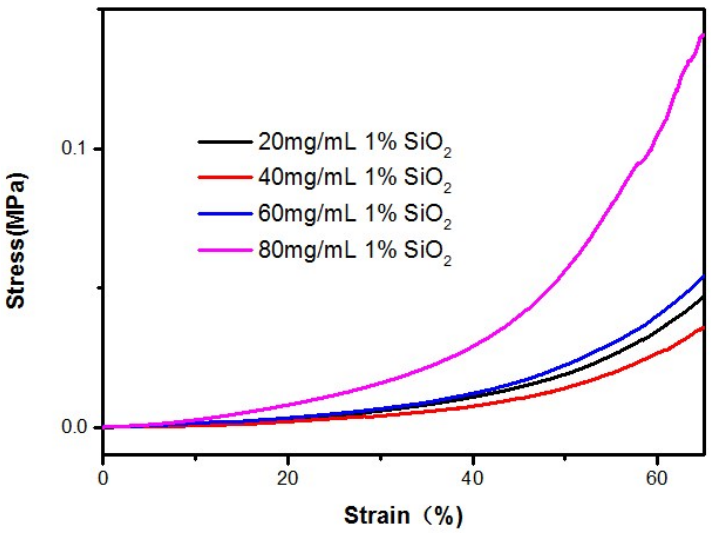

Fig. S6 Compressive strain-stress curves of the hydrogels.

Fig. S7 Photo images of the hydrogel with or without deformation.

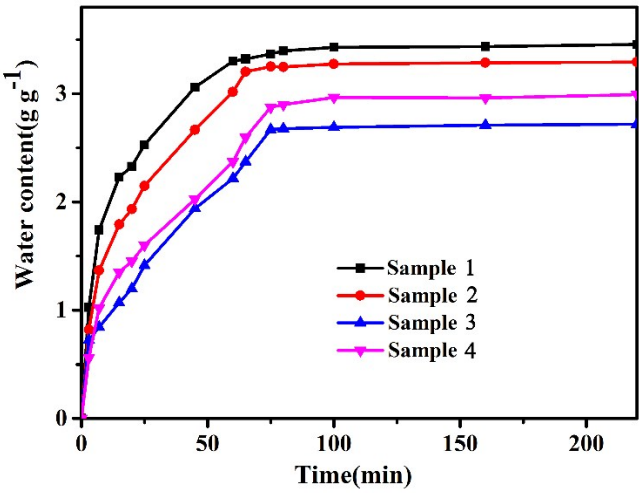

(a) sample 1-4 are hydrogels with aerogel content of 0.08, 0.16, 0.24, and 0.4 wt.%.

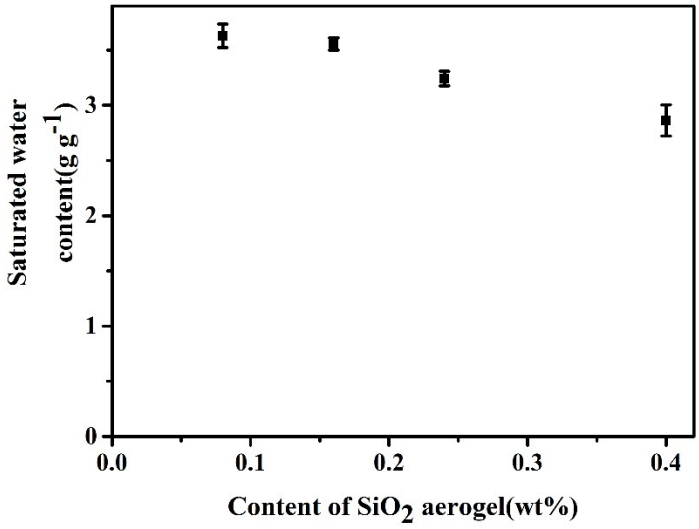

(b)

Fig. S8 (a) water evaporation rate of the functional hydrogels; (b) saturated water content of the functional hydrogels with different contents of aerogels.

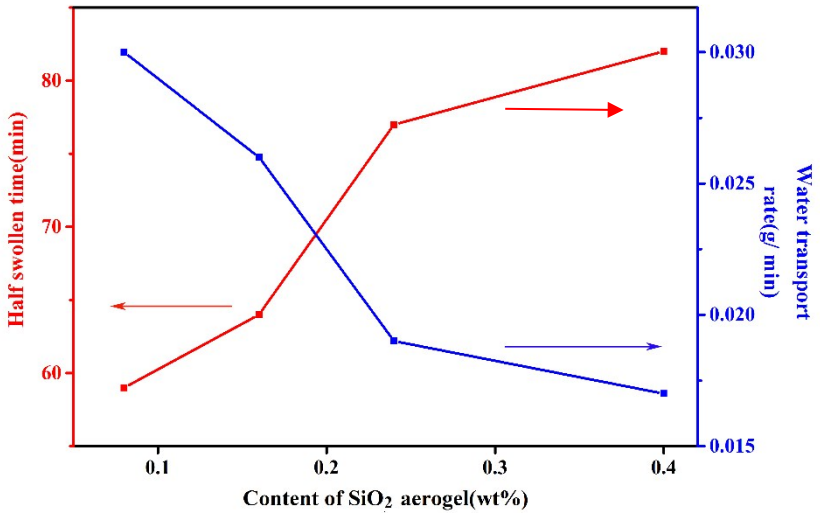

Fig. S9 swollen time and water transport rate of the functional hydrogels with different contents of aerogels.

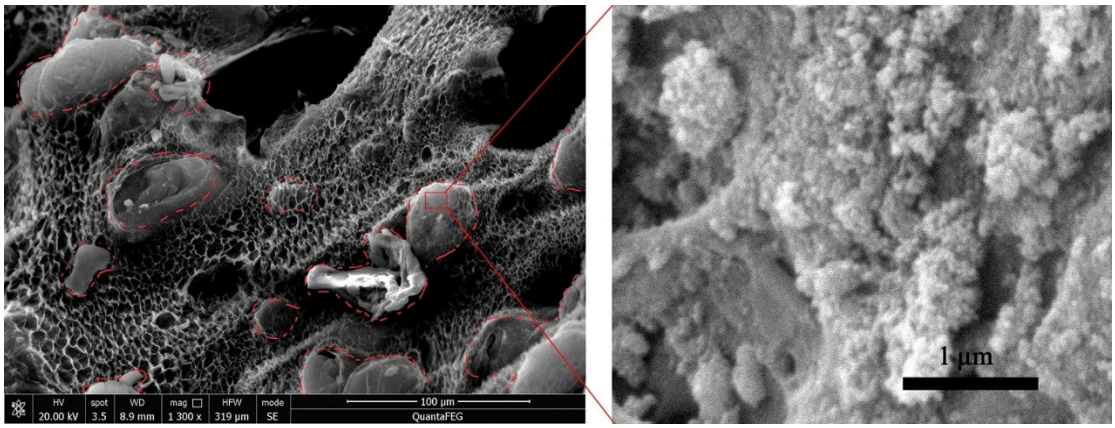

Fig. S10 SEM image of the upper side of the functional PVA hydrogel, the red circles indicate the silica aerogel microparticles embedded in the PVA matrix. From the SEM image at higher magnification times, the porous structure of the silica aerogel could be clearly identified, which indicate that the silica aerogels are intact and the PVA form the matrix but not permeate into the silica aerogels.

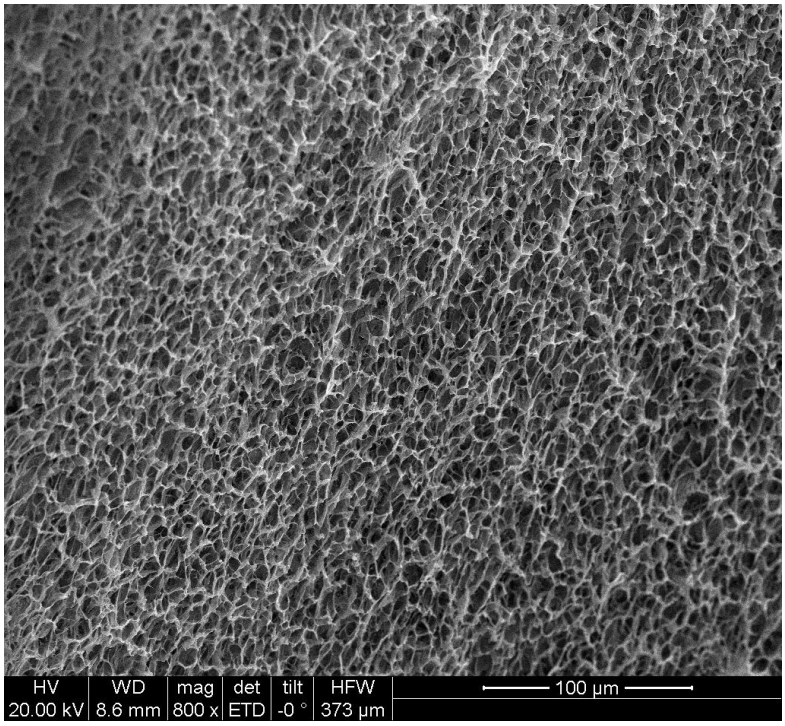

Fig. S11 SEM image of the bottom side of the functional PVA hydrogel.

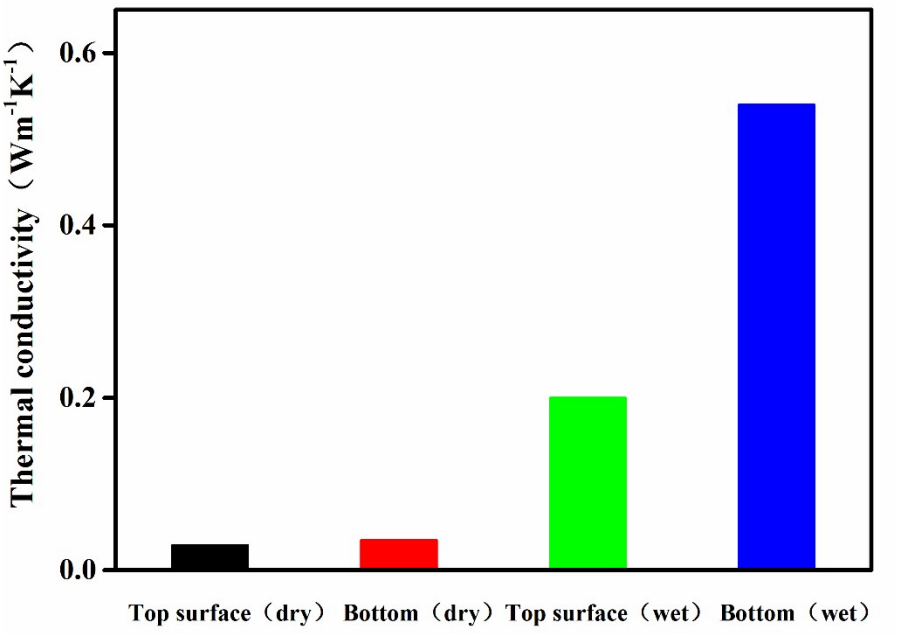

Fig. S12 Thermal conductivity of the functional PVA xerogel (dry) and hydrogel (wet).

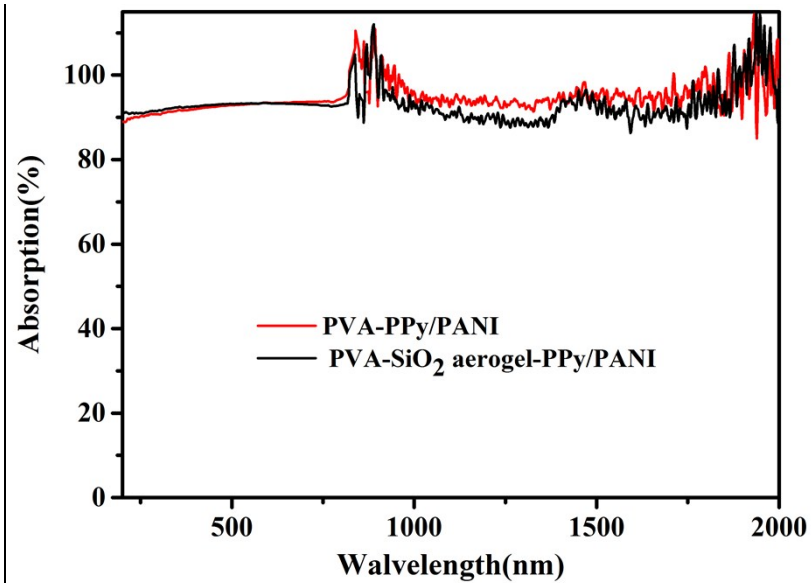

Fig. S13 Absorption spectra of the PPy-co-PANI CPHS hybrid PVA hydrogel and CPHS-aerogel hybrid PVA hydrogel.

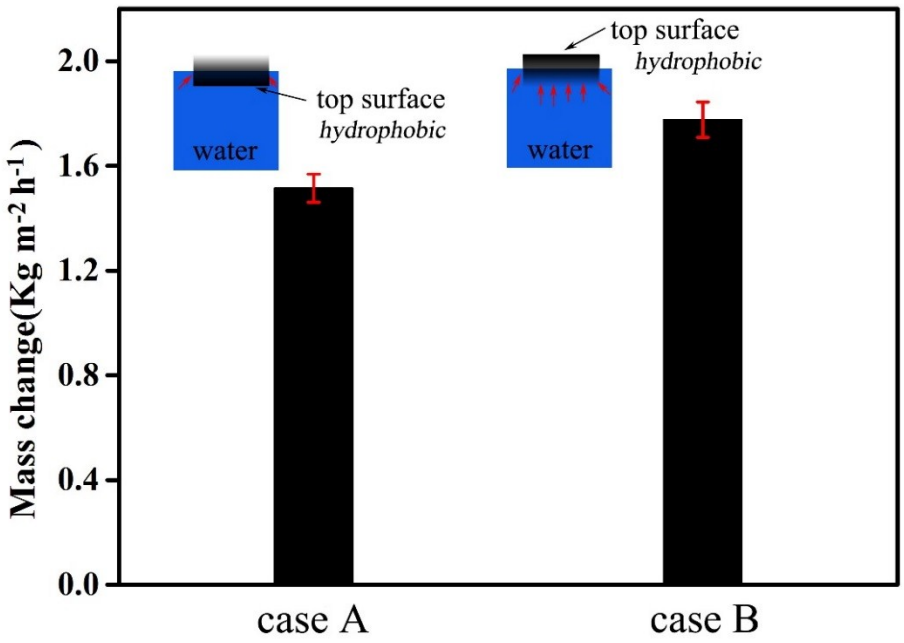

Fig. S14 ER values of water in different cases: Case A is presenting the top surface (which is hydrophopbic) in water, the hydrophobic behavior of the top surface may reduce water transportation rate to the hydrogel, thus result in lower ER of 1.52 kg/m^{2}h. Case B is presenting the bottom side in water, the hydrophilic nature and macro-size channels may facilitate the water transportation into the hydrogel, thus result in higher ER of 1.78 kg/m^{2}h. Therefore, in the present work, all the evaporation measurements were carried out by presenting the bottom side of the hydrogels in water unless it has been pointed out.

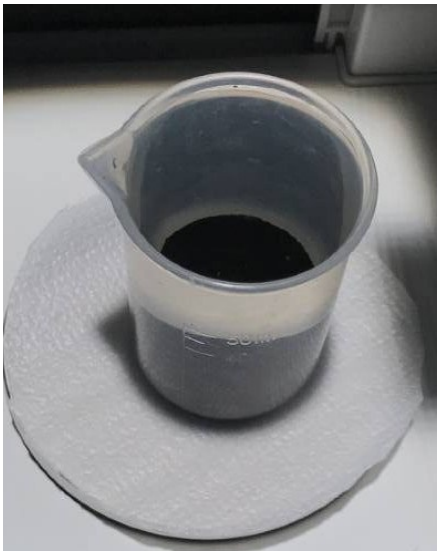

Fig. S15 Photo image of CPHS functionalized PVA hydrogels after stabilized in water. The hydrogel was black and it sink into the water bottom.

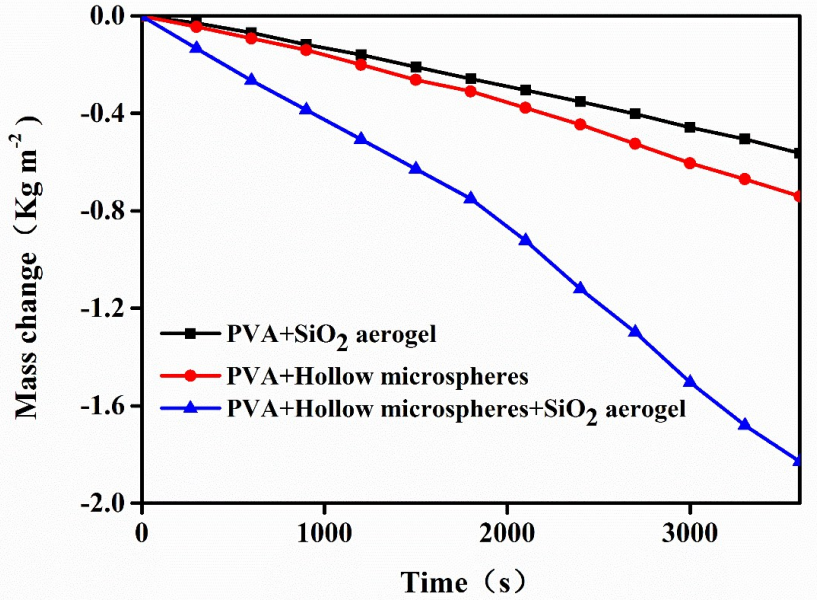

Fig. S16 Real-time water weight loss through the evaporation of the hydrogels.

Fig. S17 Photo image of aerogel functionalized PVA hydrogels after stabilized in water. The hydrogel was white and it could self-float on water.

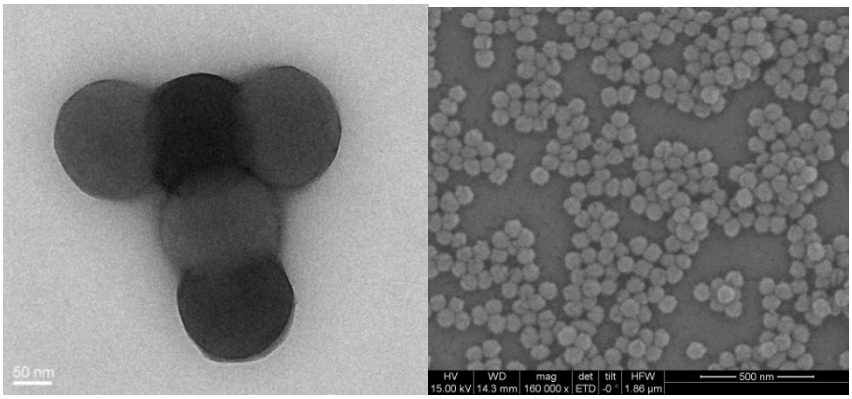

(a) PPy/PANI (b) PPy

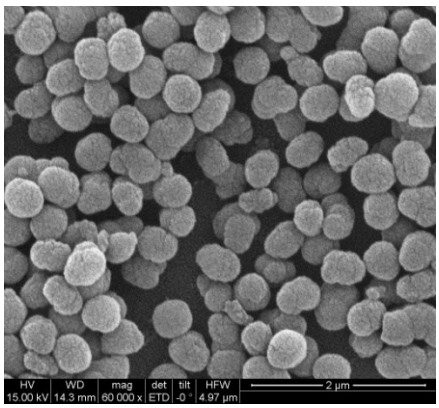

(c) PANI

Fig. S18 (a) TEM image of PPy/PANI composite conducting polymer solid spheres.

(b) and (c) SEM images of conducting polymer solid spheres as indicated.

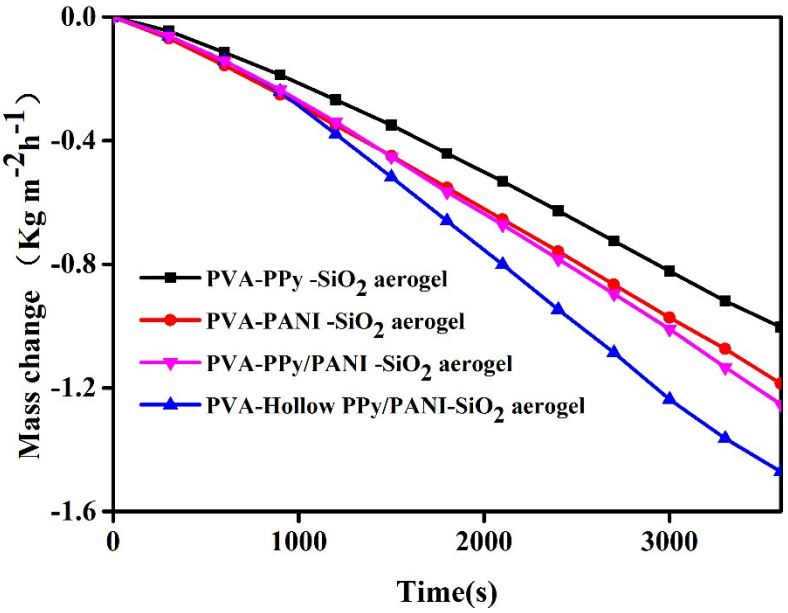

Fig. S19 Real-time water weight loss through the evaporation of the hydrogels, the thickness of the hydrogels was 3mm, and the content of solid spheres and aerogels were 1.2 wt% and 0.16 wt%, respectively.

Fig. S20 Photo image of CPHS dispersed in water.

The CPHS microspheres were presented on the water surface, they are wetted by water and became suspended in water in 10 min, few of the CPHS were floated on the water surface. The amount of water was ca. 33 ml, and the CPHS was 120 mg, which was equal to the amount of CPHS in the hydrogel content 1.2 wt.% CPHS.

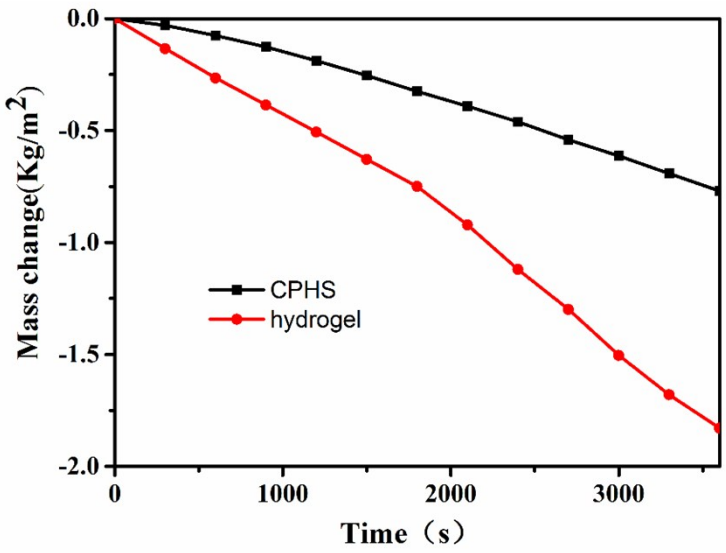

Fig. S21 Real-time water weight loss through the evaporation of the CPHS alone and the hydrogel containing CPHS (the thickness of the hydrogels was 3 mm, and the content of solid spheres and aerogels were 1.2 wt.% and 0.16 wt.%, respectively.

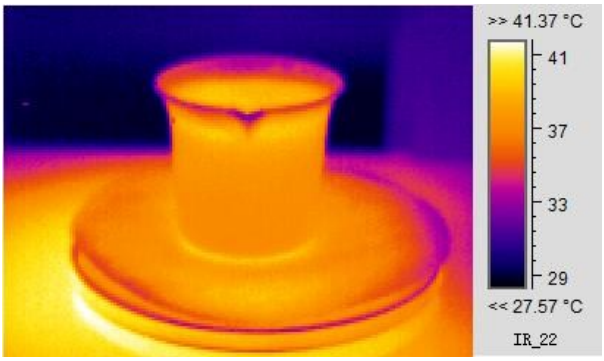

Fig. S22 Infrared photo image of the CPHS-suspended water solution under 1 Sun illumination for 30 min.

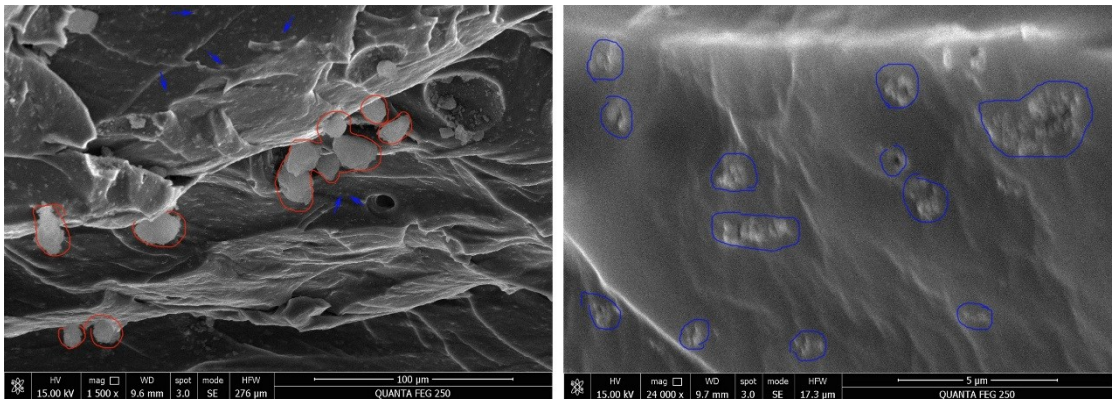

Fig. S23 SEM images of hydrogel without freeze-and-thaw treatments. The red cycles indicate the silica aerogel and the blue arrows (white spot) and blue cycles indicate the CPHS.

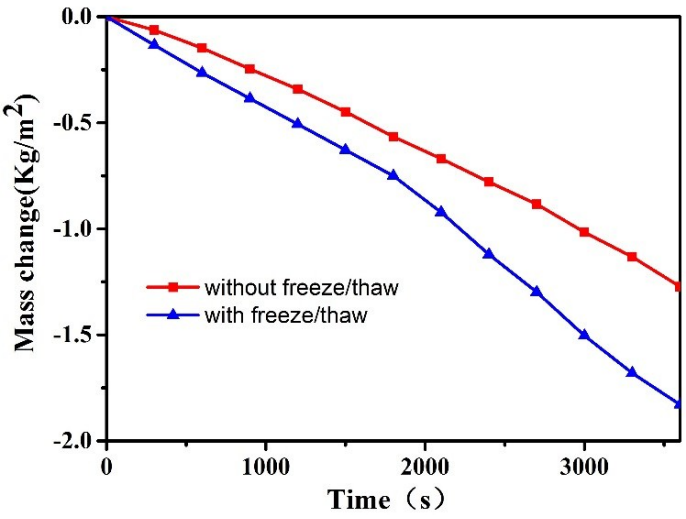

Fig. S24 Real-time water weight loss through the evaporation of the hydrogels with and without freeze-and-thaw treatment.